Scanning Microscopy Vol. 12, No. 1, 1998 (Pages 43-59) 0891-7035/98$5.00+.25
Scanning Microscopy International, Chicago (AMF O'Hare), IL 60666 USA

SCANNING PROBE MICROSCOPY OF SEMICONDUCTOR HETEROSTRUCTURES

C.K. Shih[1]*, S. Gwo[2], A.R. Smith[3], K. J. Chao[1], G. Guttroff[4] and J.W. Keto[1]

[1]Department of Physics, University of Texas, Austin, Texas 78712-1081, USA

(Received for publication June 21, 1996 and in revised form November 27, 1996)

Abstract

Atomic, electronic, and optoelectronic properties of semiconductor heterostructures are studied using scanning tunneling and near-field optical microscopes. Sample systems are AlGaAs/GaAs and InGaAs/GaAs multi-layer structures grown using molecular beam epitaxy. Real-space mapping of electronic structure including the determination of heterojunction band discontinuities is shown in AlGaAs system. In terms of the atomic structural investigations, we focus on how various growth parameters influence the interfacial abruptness in the AlGaAs/GaAs systems. Identification of different chemical constituents in the alloys and determination of atom-atom pair correlations are also demonstrated. The optoelectronic properties of AlGaAs / GaAs heterostructures are investigated using a new design of near-field optical microscope. The influence of metallurgical defects on light emission efficiency is revealed using near-field photoluminescence. In addition, local concentrations of p-type dopants and their binding energies are also resolved.

Key Words: Scanning tunneling microscopy, near-field scanning optical microscopy, semiconductor heterostructures.

[2]Current address: Department of Physics, National Tsing-Hwa University, Hsin-Tsu, Taiwan, R.O.C.
[3]Current address: Department of Physics, Carnegie Mellon University, Pittsburgh, PA
[4]Current address: Department of Physics, Wuerzburg University, Wuerzburg, Germany

*Address for correspondence:
Chih-Kang Shih
Department of Physics, University of Texas,
Austin, Texas 78712-1081, USA
Telephone number: 512 471 6603
FAX number: 512 471 1005
E-mail: shih@physics.utexas.edu

Introduction

Remarkable advances in semiconductor technology have been made possible by the ability to tailor the electronic structure of materials by stacking dissimilar materials into multilayered heterostructures. These heterostructures are the building blocks for many advanced electronic and optoelectronic devices. For example, the introduction of the double heterostructure was the key to the successful development of semiconductor lasers for room-temperature operation. The recent success of the quantum cascade laser marks another important milestone. Another application was the separation of ionized doping impurities from the charge carriers to achieve extremely high mobility (in modulation doped field effect transistors). These technological advances have also enabled studies of the quantum Hall effect (QHE) and the fractional quantum Hall effect (FQHE) manifested in quasi-two-dimensional systems and the observation of other novel quantum phenomena in lower-dimensional systems. In all cases, a detailed knowledge of the specific interfacial structures is important to be able to take full advantage of the benefits these heterostructures can offer.

In the past, transmission electron microscopy (TEM), photoelectron spectroscopy (PES), photolumi-nescence spectroscopy (PL), and cathodoluminescence spectroscopy (CL) have been utilized to study the structural, electronic and optotelectronic properties of semiconductor heterostructures. Such studies formed the foundation of conventional views regarding how these physical properties are inter-related and how they are related to the material growth parameters. Over the past few years, various forms of scanning probe microscopy (SPM) have emerged as a new set of powerful tools to investigate these properties with unprecedented spatial resolution. They are starting to provide new pictures that are complementary, or in some cases, contrary to those derived from conventional methods.

For example, applications of STM onto the cross-sectional surface [this type of approach is therefore called cross-sectional STM (XSTM)] have provided a single-sliced view of the atomic registry across hetero-structure interfaces (Albrektsen *et al*., 1990; Johnson *et al*., 1993a; Salemink *et al*., 1992; Smith *et al*., 1995a, 1995b), complementing the columnar averaged information provided by cross-sectional TEM. The

identification of different chemical constituents in the alloys and the dopant atoms provides an even more detailed view of how atoms and dopants are incorporated during the growth process (Chao *et al*., 1996a, 1996b; Johnson *et al*., 1993b; Pfister *et al*., 1995; Smith *et al*., 1996; Zheng *et al*., 1994). Tunneling spectroscopy and tip-induced luminescence spectroscopy (also applied on the cross-sectional surface) have been utilized to achieved a real-space mapping of electronic structure across the heterojunction (Feenstra *et al*., 1994; Gwo *et al*., 1993; Lew *et al*., 1994, Renaud and Alvarado, 1991). Moreover, the implementation of near-field scanning optical microscopy (NSOM) to study local photoluminescence properties have revealed new information regarding the spatial inhomogenuity of quantum well systems (Hess *et al*., 1994), contrary to the earlier view of interfacial structural properties derived from far-field photoluminescence (PL) studies.

This paper is a brief review of such efforts conducted in the authors' laboratories over the past few years. While similar efforts have been pursued in other laboratories, our intent is not to give an extensive overview here. Therefore, only experimental results from the authors' laboratory are presented here. Relevant connection to others' work will also be briefly mentioned. The paper is divided into the following sections: (**1**) a brief introduction to cross-sectional STM, (**2**) a direct mapping of electronic structures in real space, (**3**) atomic scale views of interfacial roughness, (**4**) the identification of different chemical constituents in the alloys and the atom-atom correlation, and (**5**) mapping local optoelectronic properties using near-field scanning optical microscopy.

A Brief Introduction of Cross-Sectional STM

Ever since the inception of STM, the idea of cross-sectional STM has existed and has been pursued. In 1990, the first atomic image across AlGaAs/GaAs heterojunctions was achieved (Albrektsen *et al*., 1990). Since then much progress has also been made by many other groups.

Since STM is a surface sensitive tool, it is very important to assure that the bulk properties of hetero junctions, such as band offsets, can be measured at the cross-sectional surface. In the case of III-V compound semiconductor surfaces, the intrinsic surface states lie outside of the fundamental band gap. As a result, the measured band-edge positions using tunneling spectroscopy, correspond to the bulk band-edge position (Stroscio *et al*., 1987). Moreover, the (110) surface is an unreconstructed 1x1 surface with empty surface states centered around the group m atoms and filled surface states centered around the group V atoms (Feenstra *et al*., 1987). Thus, it is possible to map out cation- and anion-sublattices independently by simply reversing the sign of the tunneling bias. These advantages make compound

Figure 1 (*on facing page*). A 7000 Å × 5000 Å STM image of $Al_{0.3}Ga_{0.7}As$/GaAs heterojunctions acquired with a sample bias of -2.35 V and a tunneling current of 0.3 nA. The upper part is the structure of $Al_{0.3}Ga_{0.7}As$/GaAs heterojunctions grown by molecular beam epitaxy (MBE) and the lower part is a line-cut across the image (position indicated by the dashed line).

---

semiconductor heterojunctions ideal candidates for XSTM/S studies. Similar approaches have been attempted on Si/Ge system, with more limited success because of the difficulties involved in producing a cross-sectional surface which represents the bulk junction.

A Direct Mapping of Electronic Structure in Real Space

Band edge discontinuities (or band offsets) are the most important parameters in bandgap engineering of semiconductor heterostructures. Measurements of band offsets have been a focus of research for many years. Albrektsen *et al*. (1990) who achieved the first atomic image of the AlGaAs/GaAs heterojunctions, also attempted the first direct measurement of band offsets. Unfortunately, the apparent valence band offset amounted to the total difference in the band gap. This result implied a zero conduction band offset which could not be possible, otherwise quantum well devices could not have existed. This inconsistency was later attributed to the tip-induced band bending effect (Salemink *et al*., 1992).

Tip-induced band bending is a well known phenomena among researchers who perform tunneling spectroscopy in large gap semiconductors. In the case of homogeneous GaAs, this problem can be overcome by using highly doped samples where the high carrier density screens the field within a short length. However, in AlGaAs/GaAs heterojunctions, even when both AlGaAs and GaAs are doped degenerately, there exists a depletion region, right at the area of interest (due to the band offset), which inevitably produces a severe tip-induced band bending. In our earlier work (Gwo *et al*., 1993), we found that by passivating the cleaved surface with sulfide solutions, the surface Fermi level was uniformly pinned. Since the extrinsic surface states that pin the Fermi level also screen out the electrical field, tip induced band bending is avoided. Feenstra *et al*. (1993) reported a similar situation on a highly stepped surface with the Fermi level also strongly pinned.

Figure 1 shows a filled-state STM image of a sulfide-passivated cross-sectional surface of AlGaAs/-GaAs heterostructures. The corresponding growth structure is displayed above it. The GaAs buffer layer shown in the image allows an unambiguous assignment of the GaAs and (AlGa)As

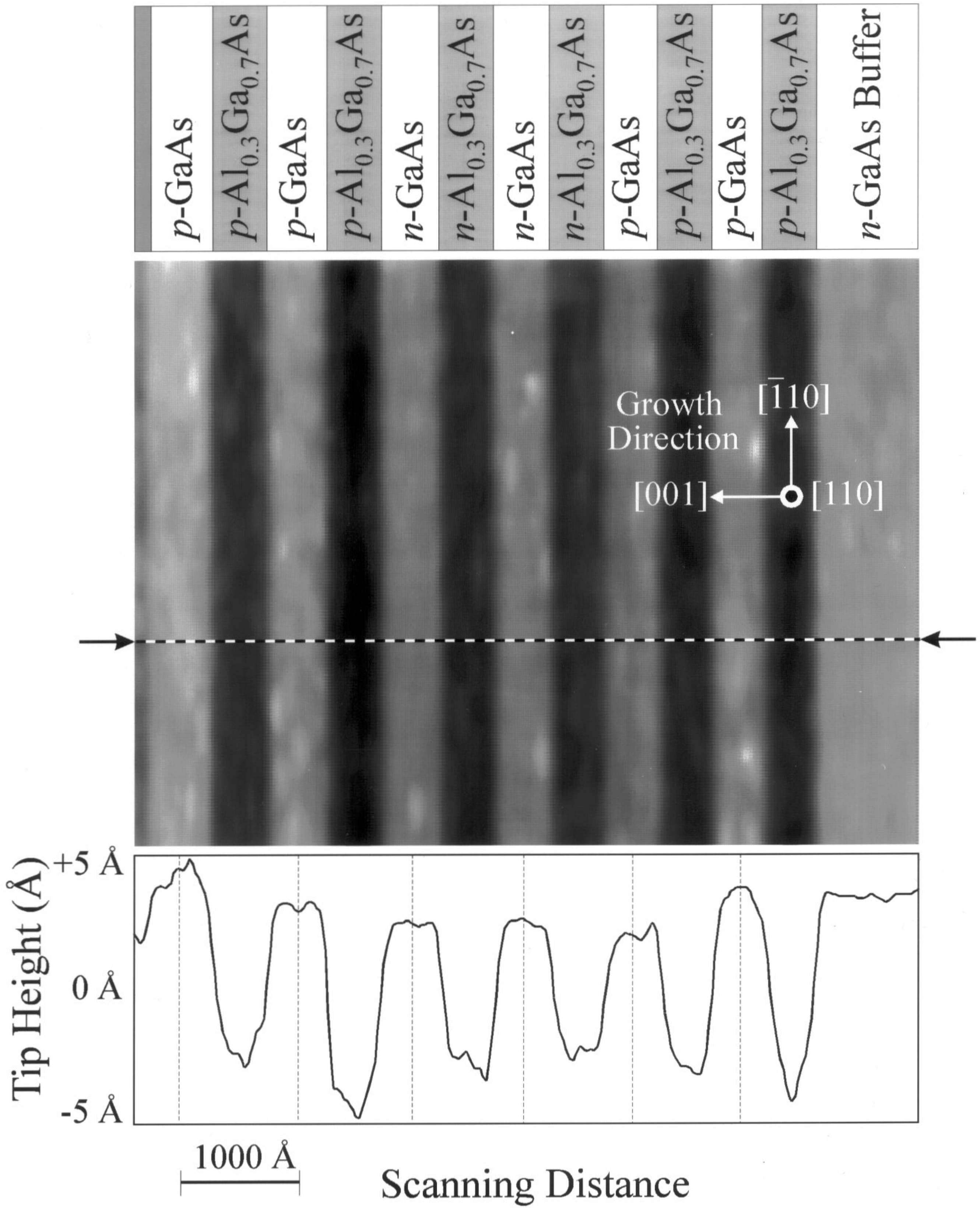

p-GaAs
p-Al0.3Ga0.7As
p-GaAs
p-Al0.3Ga0.7As
n-GaAs
n-Al0.3Ga0.7As
n-GaAs
n-Al0.3Ga0.7As
p-GaAs
p-Al0.3Ga0.7As
p-GaAs
p-Al0.3Ga0.7As
n-GaAs Buffer
Growth Direction
[$\bar{1}$10]
[001]
[110]
Tip Height (Å)
+5 Å
0 Å
-5 Å
1000 Å
Scanning Distance

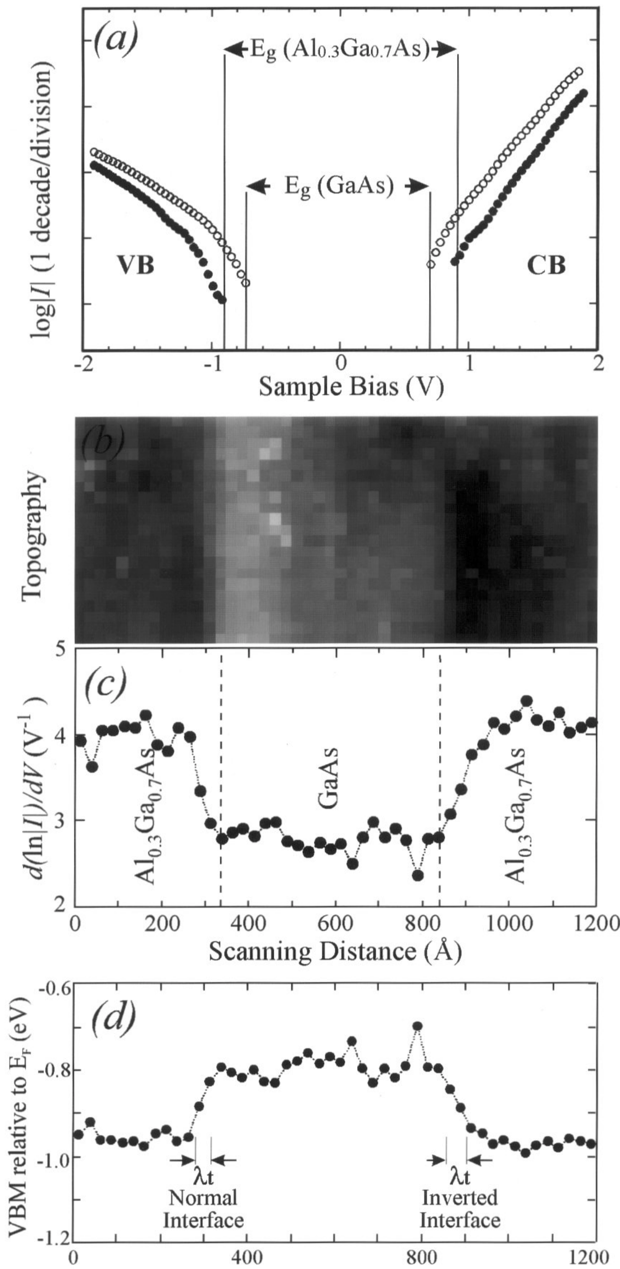

Figure 2. (**a**) Two representative spectra acquired at GaAs (open circles) and AlGaAs (filled circles) regions. (**b**) A 48 × 21 pixel STM image in which tunneling *I-V* (current-voltage) spectra were taken at each pixel in the image. (**c**) Plot of normalized conductivity (d(ln | I |)/dV) (derived from tunneling *I-V* spectra) versus position at a negative sample bias (1.59 V). Each data point in this plot represents the averaged result from the *I-V* spectra along the y-direction. (**d**). The positions of valence band edges (referenced to the Fermi level) across the $Al_{0.3}Ga_{0.7}As$/GaAs heterojunctions determined by the (d(ln | I |)/dV) versus x plot at a sample bias of 1.59 V.

Figure 3. (*on facing page*) (**a**) and (**b**). Tunneling *I-V* spectra acquired on a sulfide passivated GaAs (110) surface and on a UHV-cleaved GaAs (110) surface. (**c**) and (**d**). The tunneling *I-V* spectra with the sample biased positively (tunneling into empty states) in GaAs and $Al_{0.3}Ga_{0.7}As$ regions, respectively. The vertical scale for $Al_{0.3}Ga_{0.7}As$ has been scaled down by a factor of 0.4. The dots are experimental data and the solid curves are fitted spectra. **Insets** in (c) and (d) correspond to the numerical derivative, dI/dV, of the *I-V* spectra.

---

regions. From the line-cut shown below, one finds that (AlGa)As regions appear deeper than GaAs regions by about 5 Å. The deeper appearance of the (AlGa)As regions is primarily an electronic effect. It should be noted that the sulfide passivation procedure used here is very different from the one used in Dagata *et al*. (1992) where preferential etching on AlGaAs was found.

Tunneling spectra were acquired on 64 × 64 pixel images where *I-V* tunneling spectra were recorded at each pixel by interrupting the STM feedback. Two representative spectra acquired in GaAs and (AlGa)As regions are shown in Figure 2a which show gap values of 1.4 ± 0.1 and 1.8 ± 0.1 V, respectively. The pinning of the Fermi level at the surface is evident from the spectra. Figure 2b shows a 48 × 21 pixel image which covers a region of *p*-$Al_{0.3}Ga_{0.7}As$/p-GaAs/-p-$Al_{0.3}Ga_{0.7}As$. While most of the important spectroscopic information is contained in these *I-V* spectra, extraction of the useful information is non-trivial. Such a large set of spatially resolved spectra were analyzed by a normalized conductivity (d(ln | I |)/dV) method which provides a "parameter free" procedure to extract important information.

The reason to use (d(ln | I |)/dV) is two fold. First of all, this quantity is independent of the tip to sample separation {same as (dI/dV)/(I/V)}. Since the topographic contrast between AlGaAs and GaAs results from an electronic effect, the absolute tip-to-sample distance varies from the GaAs to the AlGaAs regions. Using this quantity completely removes this effect. Secondly, if the tunneling current has a power law dependence of the form $I \sim (V-V_0)^{\alpha}$ near the band threshold where V_0 is the threshold and α a fitting exponent, then $d(\ln|I|)/dV = \alpha/(V-V_0)$, showing a $1/(V-V_0)$ dependence (Gwo *et al*., 1993). As a result, the closer to the band edge, the larger this normalized conductivity is. Spatial variation of d(ln | I |)/dV, therefore, reflects spatial variation of V_0. Indeed, as shown in Figure 2c, a larger value of d(ln | I |)/dV is found in the (AlGa)As region, indicating the existence of a valence band offset (VBO) (Gwo *et al*., 1993).

One can further determine the power law exponent α by fitting d(ln | I |)/dV versus V. This number then allows one to plot V_0 as a function of the scanning position as the one shown in Figure 2d. The band offset can, therefore, be

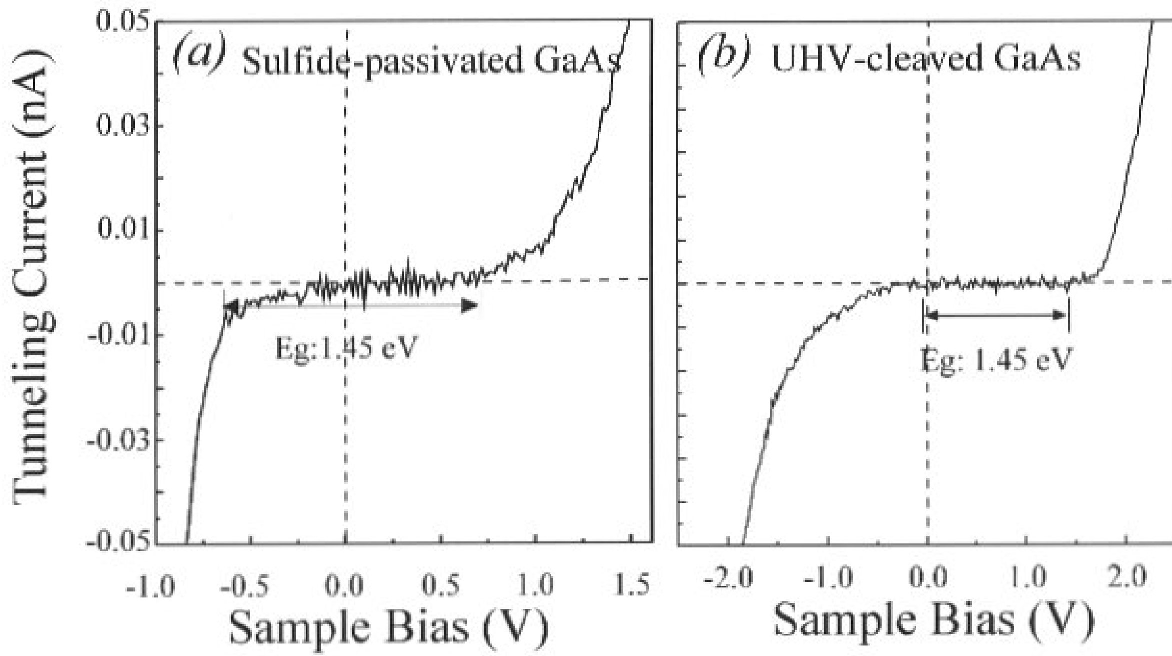
(a) Sulfide-passivated GaAs
Eg:1.45 eV
(b) UHV-cleaved GaAs
Eg: 1.45 eV
Tunneling Current (nA)
0.05
0.03
0.01
-0.01
-0.03
-0.05
-1.0
-0.5
0.0
0.5
1.0
1.5
-2.0
-1.0
0.0
1.0
2.0
Sample Bias (V)
Sample Bias (V)

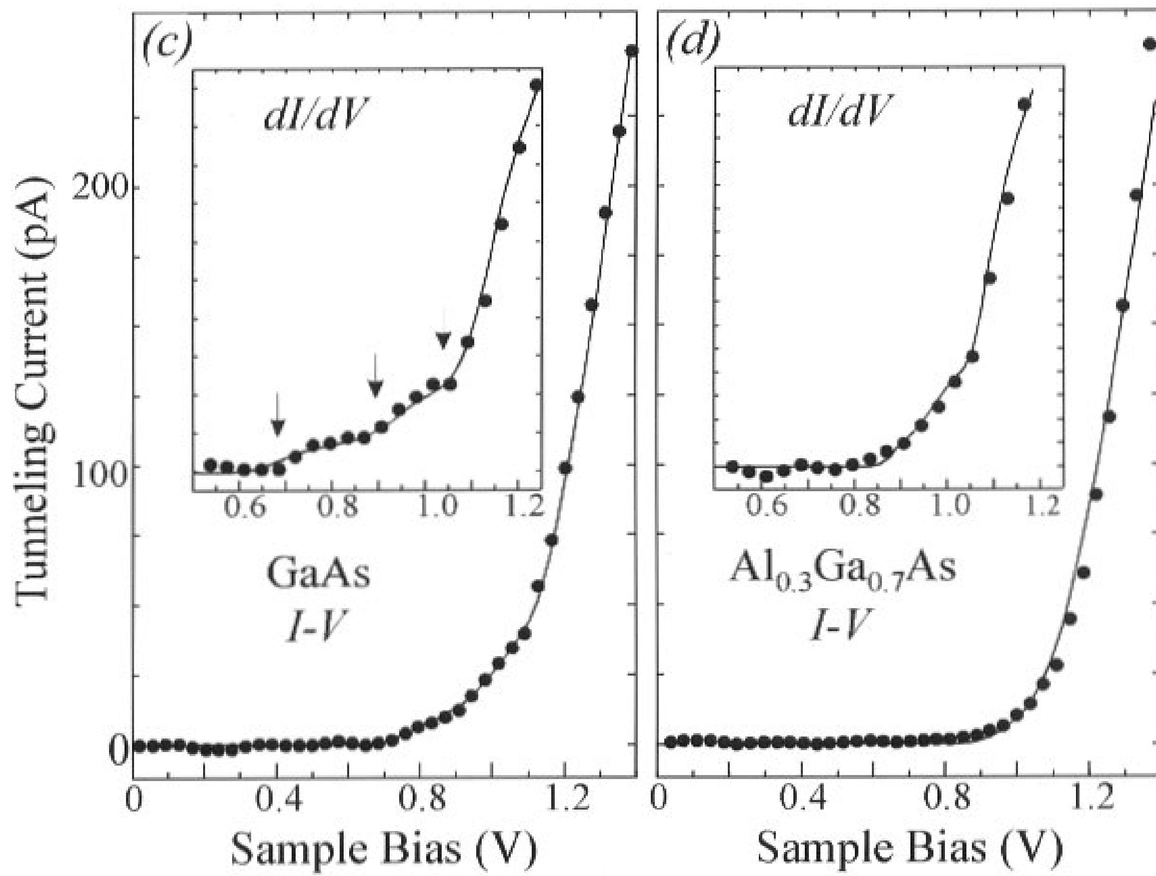
(c)
(d)
dI/dV
dI/dV
GaAs
I-V
Al0.3Ga0.7As
I-V
Tunneling Current (pA)
200
100
0
0.6
0.8
1.0
1.2
0
0.4
0.8
1.2
Sample Bias (V)
Sample Bias (V)

determined to be 0.17 eV. Also shown in this plot is the asymmetry in the transition widths at the two inequivalent interfaces: AlGaAs-on-GaAs versus GaAs-on-AlGaAs. This was interpreted to be due to the asymmetry in the interfacial roughness (Gwo *et al*., 1993).

It is clear that the pinning of the Fermi level at the surface is due to the existence of extrinsic surface states created by our sulfide passivation procedure (our procedure, therefore, is not a good electrical passivation). Figures 3a and 3b show the *I-V* curves acquired on sulfide passivated and ultra high vacuum (UHV)-cleaved GaAs (110) surfaces, respectively. The finite slope in the gap region of the *I-V* curve of the sulfide passivated sample is due to these extrinsic surface states. In addition, one also observes a signature of multiple kink structures on the conduction band spectrum which represent the multiple thresholds at the k-space points Γ, L, and X in the conduction band of GaAs. In contrast to the UHV cleaved surface, the bulk related band existed only as a small tail within a very small energy window near the band edge. Above this edge, the intrinsic surface states dominate the tunneling spectrum, totally masking the multiple band thresholds of the bulk band structure. Figures 3c and 3d show the *I-V* spectra of sulfide passivated GaAs and AlGaAs after signal averaging over about 1000 spectra where the numerical derivatives are also shown. The multiple-kink structures are more enhanced in the derivatives. One observes three thresholds in the GaAs spectrum and only two thresholds in the AlGaAs spectrum. This is because the energy locations of the L and X thresholds in AlGaAs are very close. For some other III-V semi-conductors, where the intrinsic surface states are higher above the conduction band minimum, it has been shown that multiple-band thresholds can be observed directly on cleaved surfaces using tunneling spectroscopy (Feenstra, 1994).

One very appealing application of the real space mapping of electronic structure is to directly measure the confined quantum states in quantum heterostructures. For most semiconductor quantum wells, where the size quantization of the energy level is on the order of a few to a few tens of meV, such measurements need to be performed at low temperatures. In the case of InAs/GaSb, because of a large conduction band offset, the energy separation of confined quantum well states is large enough to be observable at room temperature, as nicely demonstrated by Feenstra *et al.* (1994).

Interfacial Roughness: Atomic Scale View Versus Columnar Averaged View

For low dimensional heterostructures, interfacial roughness plays a critical role in influencing the electronic, transport and optical properties. Cross-sectional TEM has been used for many years to study this issue. However, the chemical distinguishability of TEM relies on very complicated simulation of the lattice image. In addition, the information obtained is only a columnar average over the thickness of the sample.

On the other hand, cross-sectional STM provides a single-slice view of the atomic structure across the heterostructure, thus, enabling a true atomic scale view. It should be realized that in order to define the interfacial roughness in AlGaAs/GaAs system, one needs to define a length scale over which the alloy composition can be defined. In the previous section, we discussed the asymmetry of the interfacial roughness at the normal versus the inverted interfaces of GaAs/AlGaAs heterostructures based on the electronic transition width. In that case, since we average *I-V* spectra along [110] over about 50-200 Å before deducing $(d(\ln|I|)/dV)$, this is the length scale over which our alloy composition is defined.

In the case of AlAs/GaAs without the tenary alloys, such an ambiguity is avoided. Figure 4a shows a filled- state STM image of a AlAs/GaAs short period super-lattice with the intended growth structure shown above. At each interface between AlAs/GaAs, a growth interrupt of 30 seconds was performed to improve the interfacial abruptness. On the left hand side of the short period lattice is the AlGaAs alloy region. While the image represents the As-sublattice, the local apparent height is related to the local bonding configurations to the cations. Qualitatively, the more Al atoms the As is bonded to, the lower that apparent topographic height. In the AlGaAs alloy region, atomic scale fluctuation is still observed. In the short period superlattice region, while the signature of the periodic structure is also observed, the interface is far from ideal with an inter-mixing on the order of about one unit cell.

Figures 4b and 4c show two topographic line profiles: one represents an averaged line profile along the $[\bar{1}10]$ direction (Fig. 4b), while the other represents the dashed line

Figure 4. (*on facing page*) (**a**). A 450 Å × 290 Å constant-current STM image of 23 Å GaAs/11 Å AlAs (4/2) superlattice acquired with a sample bias of 2.25 V and a tunneling current of 0.2 nA. The total gray scale for the image is about 1.5 Å. On the left, following the last 23 Å GaAs region, is a region of $Al_{0.3}Ga_{0.7}As$. (**b**). Averaged line cut across the image in Figure 4a. The averaged height difference between GaAs and AlAs is typically about 0.7 0.8 Å with atomic corrugation of about 0.08 Å. Solid arrows indicate peak positions which agree with the intended device structure. Dashed arrows indicate the expected positions of peaks which appear shifted from their correct location. This shift indicates that a single unit cell has been lost during the growth near the position indicated. (**c**). Single line cut across the image of part (Fig. 4a) showing that the superlattice is well-defined at the atomic scale.

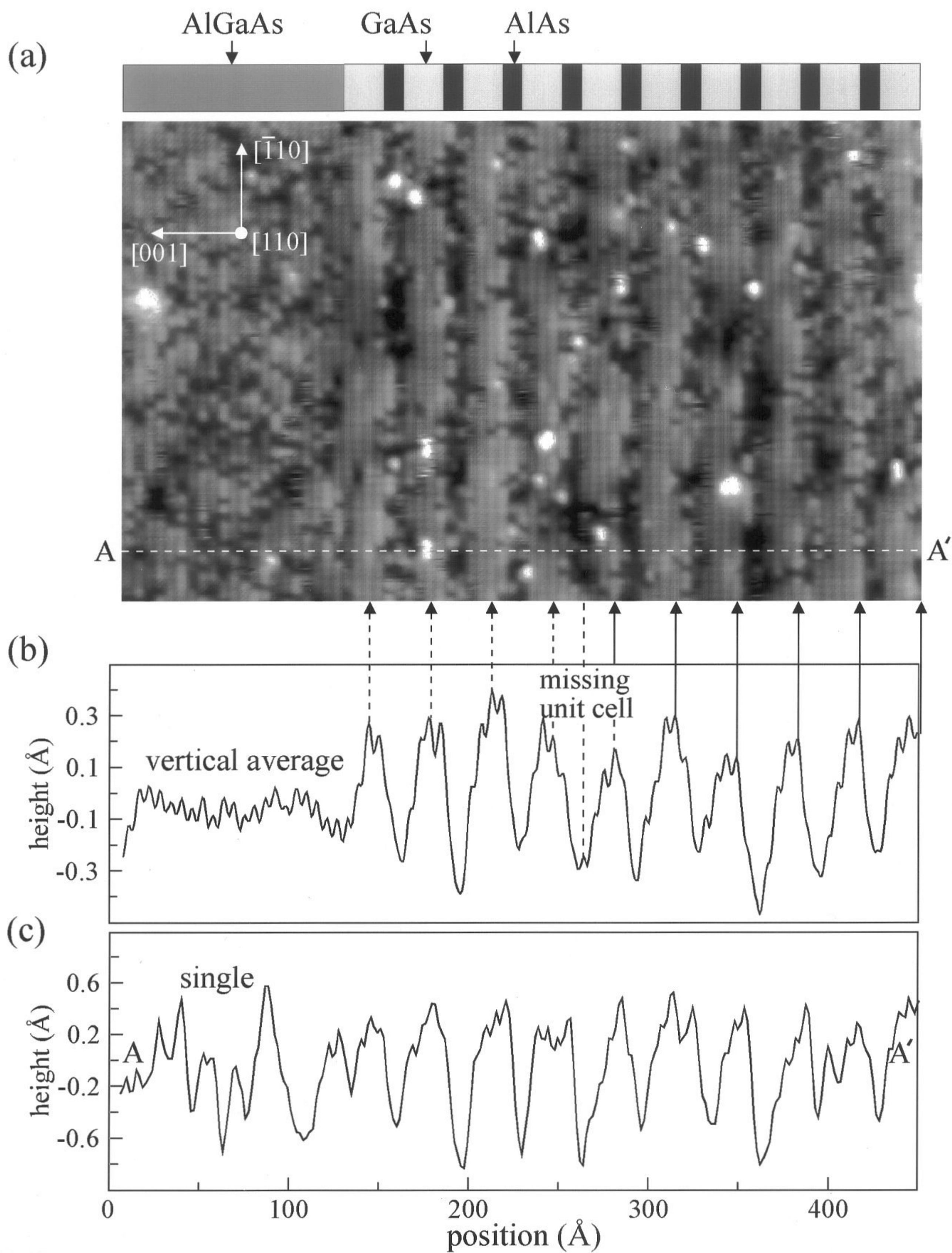

(a)
AlGaAs
GaAs
AlAs
[$\bar{1}$10]
[001]
[110]
A
A′
(b)
missing
unit cell
vertical average
height (Å)
0.3
0.1
-0.1
-0.3
(c)
single
height (Å)
0.6
0.2
-0.2
-0.6
A
A′
0
100
200
300
400
position (Å)

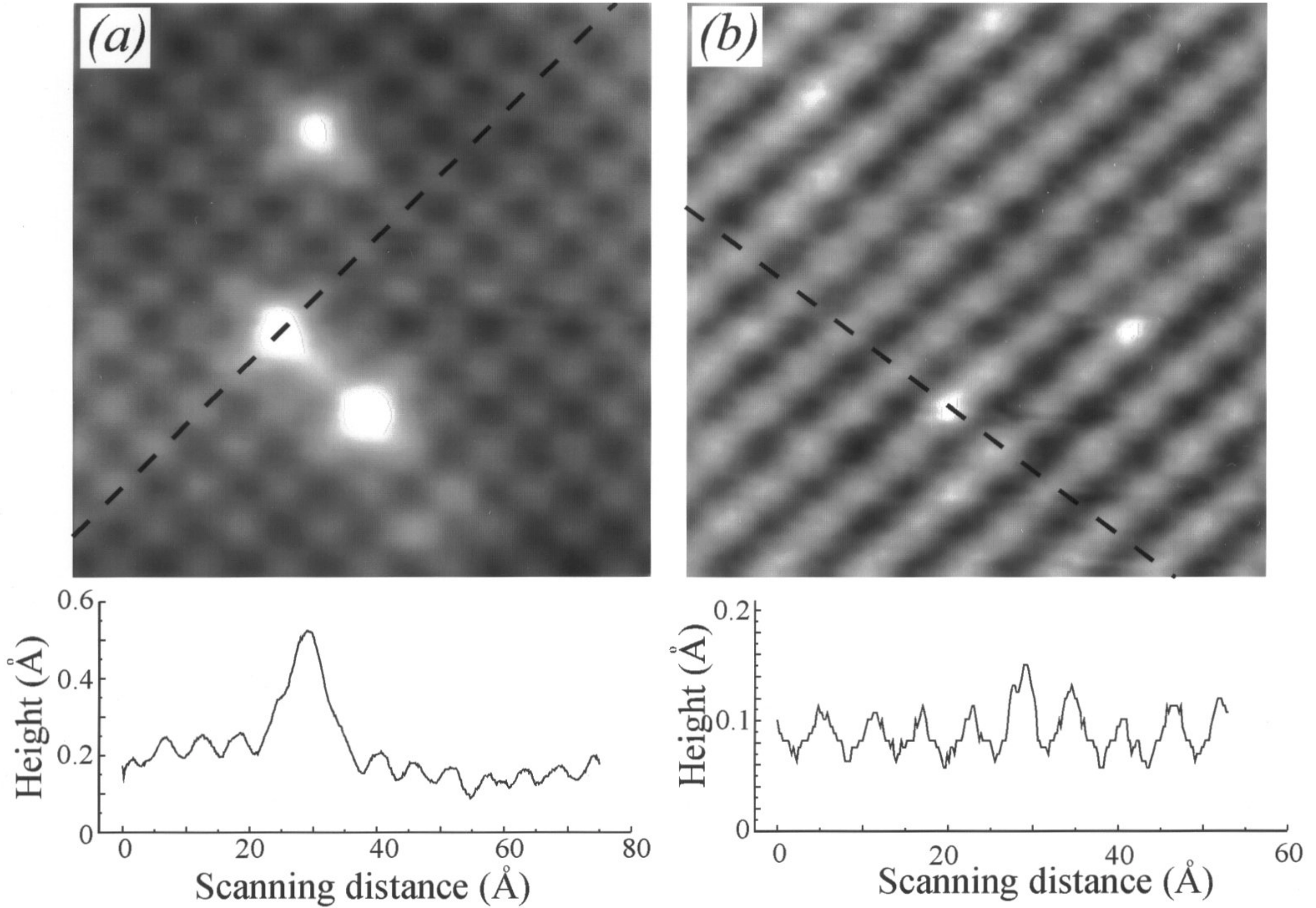

Figure 5. (**a**). Empty-state image of $In_{0.02}Ga_{0.98}As$ acquired at a sample bias of -2 V. The bright lattice sites are the locations of In atoms on the surface. The line profile across one of them is shown below. (**b**). Filled-state image of $In_{0.02}Ga_{0.98}As$ acquired at a sample bias of +2 V. The bright lattice sites are the locations of As atoms bonded to second layer In atom. The line profile across one of them is shown below.

shown in the image. The atomic scale fluctuation in the alloys region and the non-ideal interface in the superlattice region are well represented in the single line profile (Fig. 4c). After an average of about 200 Å along the $[\bar{1}10]$ direction, the atomic scale fluctuation in the alloy region is now seen as a more well-defined alloy composition, and the non-abrupt interface appearing in the single line profile is now averaged to present nice periodic structure of the short-period superlattice. This comparison of a single line profile versus the averaged line profile along the interface is particular illuminating. By performing the STM line profile average along the $[\bar{1}10]$, one simulates the columnar averaged effect of the TEM, thus, averaging out atomic scale fluctuation in the alloy and the interface roughness.

Using the average line cut, we can extract other information from the data as well. For example, for the first six periods from the right, the first GaAs layer within a single period shows up as the first small peak on the hill seen in the average line cut. The positions of these peaks are marked by the equally-spaced solid arrows in the figure which point to the corresponding rows in the image. After the sixth period, we observe an effect which is very difficult to see in the image or any single line cut. While the spacing of all the arrows remains the same across the entire superlattice, the dashed arrows point to the second row within the GaAs part of each superlattice period. This indicates a shift to the right of the last four periods by one row suggesting that a row was lost somewhere between the sixth and seventh periods of the superlattice. This appearance of a missing row over the imaged area is a local effect, and is probably due to the fluctuation of the surface step heights over the length scale of a few hundred Angstroms.

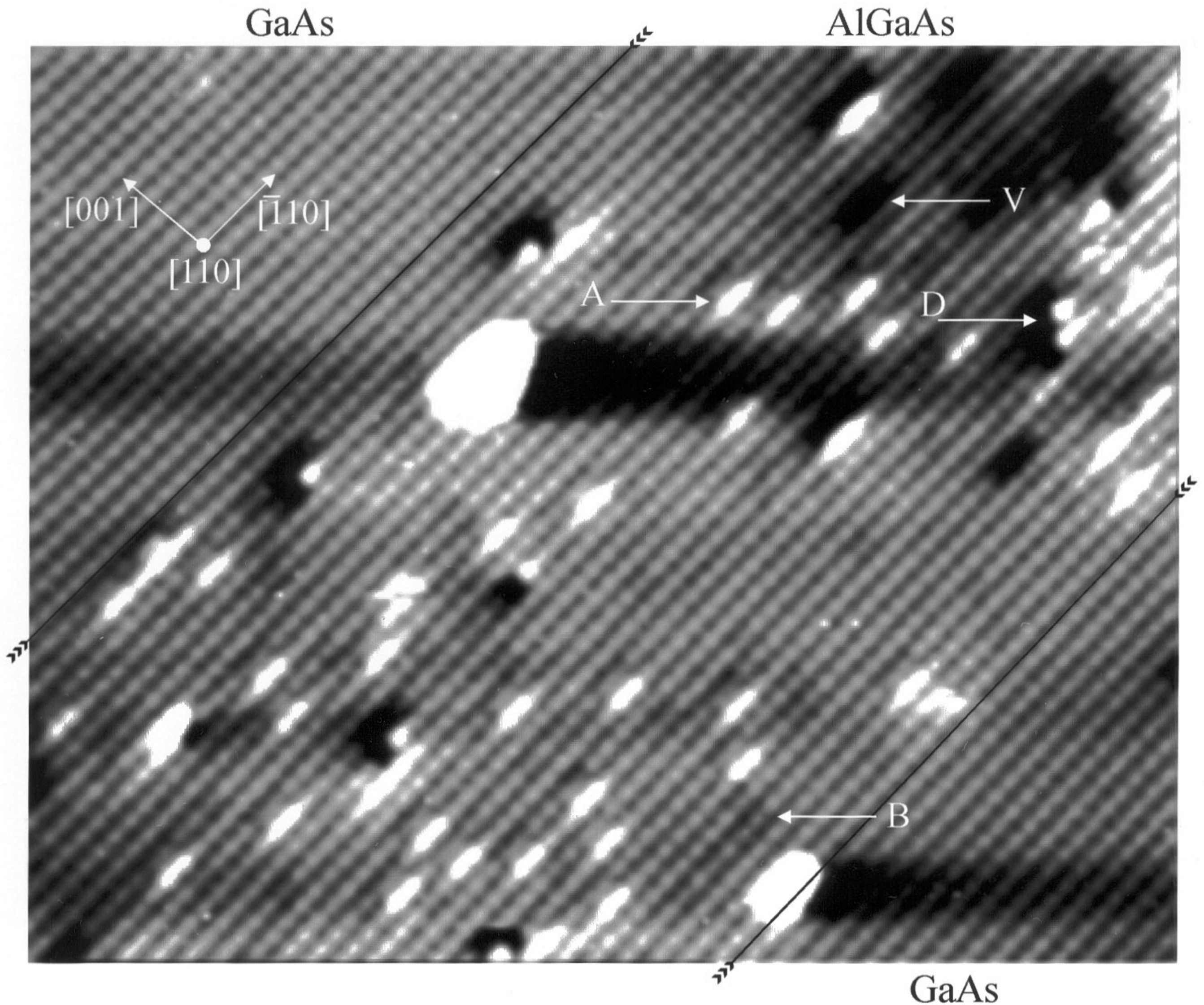

Figure 6. A 300 Å × 230 Å filled-state STM image of GaAs/$Al_xGa_{1-x}As$/GaAs heterojunction region. This image was acquired with a sample bias of -2.50 V and a tunneling current of 0.15 nA. The approximate heterojunction locations are indicated by black lines. "**A**" indicates a first layer aluminum atom feature while "**B**" indicates a second layer aluminum atom feature. Arsenic vacancies ("**V**") and other defect-related features "**D**" are also present.

Identification of Chemical Constituents and Atom-Atom Correlation in the Alloys

As mentioned above, the chemical distiguishability of the TEM technique relies on very complicated simulation of the lattice image. Furthermore, it provides only an averaged information over the thickness of the sample. Chemical distinguishability of cation versus anion atoms in compound semiconductors using STM was achieved many years ago (Feenstra *et al*., 1987). Recently, it has been demonstrated that different iso- valent cations in the common anion alloys (such as In versus Ga in InGaAs alloys, and Al versus Ga in the AlGaAs alloys) are also distinguishable (Salemink and Albrektsen, 1993; Zheng *et al*., 1994; Pfister *et al*., 1995). The distinguishability of cations in the empty-state image is understandable since the energy location of local cation surface states can differ. On the other hand, even in the anion-sublattice imaging (filled-state image), the different local bonding to the cations also gives rise to different contrast. By employing symmetry arguments, one can further locate

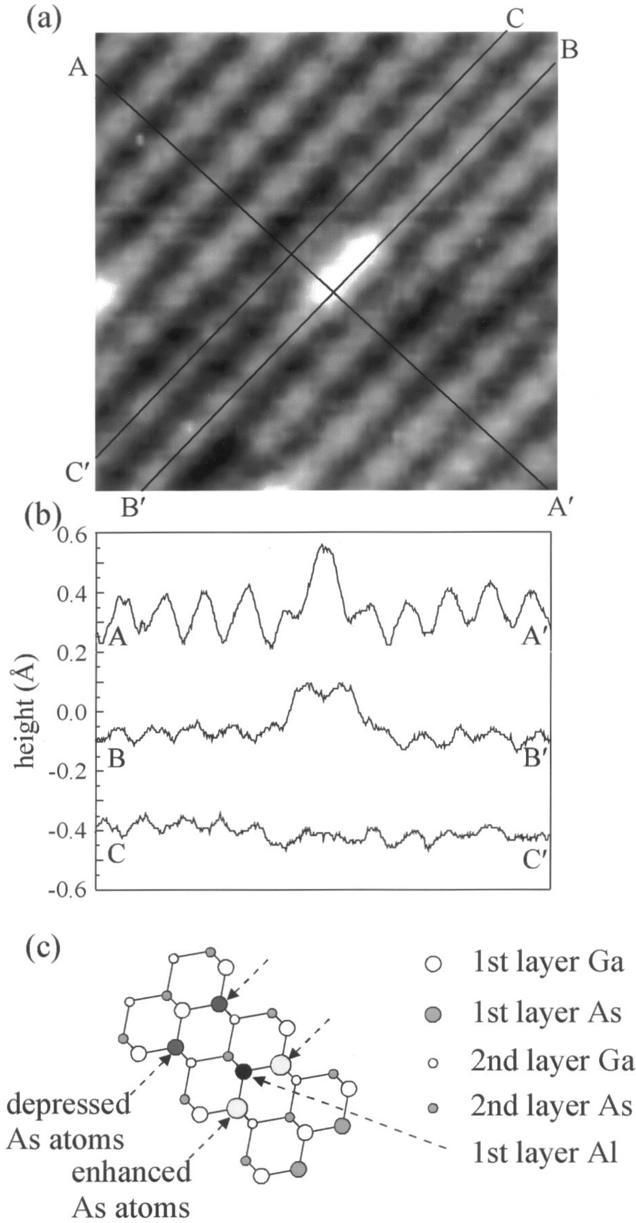

Figure 7. (**a**). Zoom-in view of the first layer aluminum feature. (**b**). Line profiles taken across the feature from the points A, B, and C to the points A', B', and C', respectively. Note that the lateral distance scales along the three line profiles are not exactly the same, but the vertical scales are the same. Line profiles have also been vertically shifted for clarity. (**c**). Atomic model of the region of the substitutional aluminum atom.

Figure 8. (*on facing page*) (**a**). Zoom-in view of the back-bonded aluminum feature which is much easier to see in the gray-scale enhanced view shown in Figure **8b**. Line profiles across the feature from the points D and E to the points D' and E' are shown in Figure **8c**. The apparent depression due to the aluminum substitution is fairly weak, only about 0.04 Å. (**d**). An atomic bonding model for the back-bonded aluminum atom is shown.

different cations on the surface and in the second layers.

Figure 5a is an example of an empty-state image of InGaAs with a nominal 2% In concentration. The bright lattice spots are interpreted to be the surface In atoms positions. The distinguishability of cations in the empty-state image is understandable since the energy location of the local cation surface states differs, and a lower band gap energy E_g of InAs implies a lower energy location of the cation surface state for In. Furthermore, the observed concentration also agrees with the nominal In concentration. Such an interpretation was first used by Zheng *et al*. (1994) and subsequently by Pfister *et al*. (1995).

On the other hand, bright spots in the filled state image are also observed with a concentration consistent with the nominal In concentration. Following the interpretation of Pfister *et al*. (1995), this feature indicates that an As atom is bonded to an In atom in the second layer. Due to the longer bond length of In-As, the second layer In will raise the physical location of the As to which it is bonded. With the data that we have obtained so far, we found that the topographic height of this feature is about 0.15 ± 0.03 Å and shows little voltage dependence within the bias range of -2 to -2.5 V. This result supports the interpretation that this feature is a true geometric effect due to the larger In-As bond length.

The identification of Al atoms in the AlGaAs alloys is slightly different than that of In in the InGaAs alloys. In our experience, it is more difficult to directly image the locations of surface Al atoms using the empty state imaging mode although we noted that Salemink and Albrektsen (1993) have done so. Nevertheless, we found that it is still possible to distinguish the locations of the surface and second layer Al atoms based on filled state images.

Figure 6 shows a 300 Å × 230 Å image of an $Al_{0.05}Ga_{0.95}As$ acquired with a sample bias of -2.50 V and a tunneling current of 0.15 nA. Throughout the image, we see a variety of different features which are characteristic of the AlGaAs region. First of all, we see a large number of elongated bright features which we refer to as "**A**" in Figure 6. Notably, the orientation of these **A** features is always the same relative to the underlying GaAs lattice. The second type of feature within the AlGaAs region is a single arsenic site which is slightly depressed relative to the surrounding arsenic atoms which we refer to as "**B**" in Figure 6. The number of these **B** features is about the same as the number of **A** features. Since

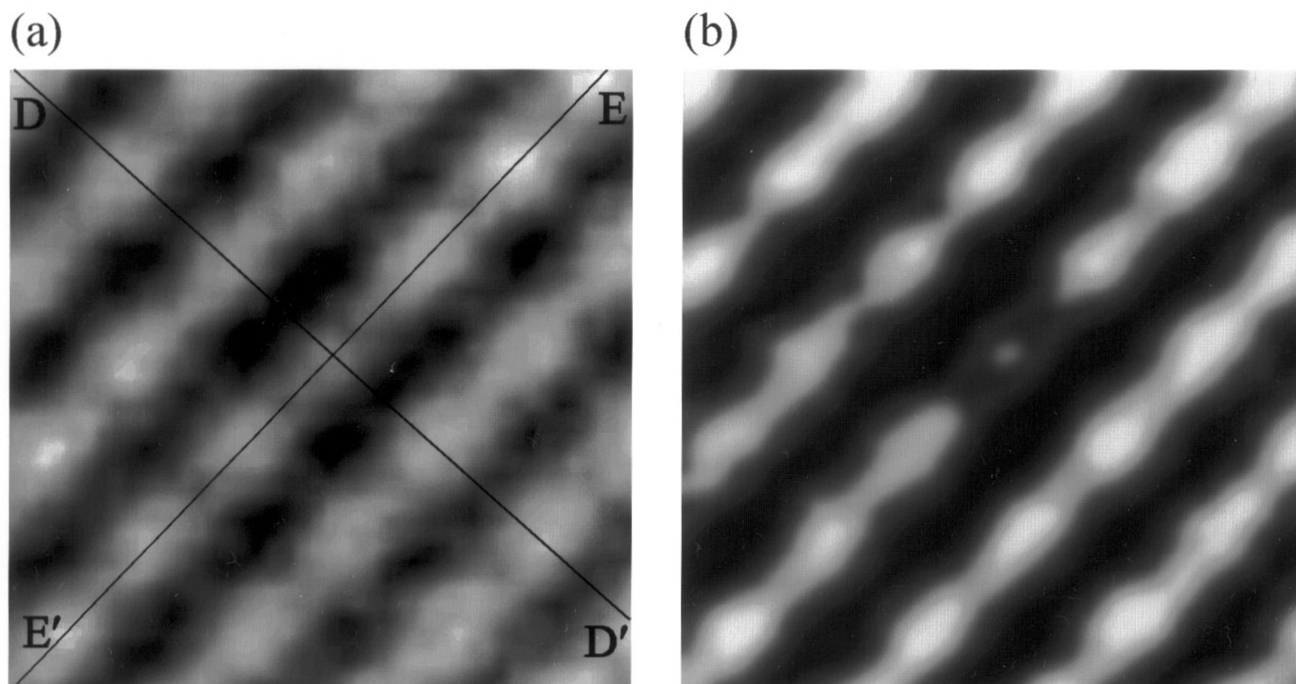
(a)
(b)
D
E
E′
D′

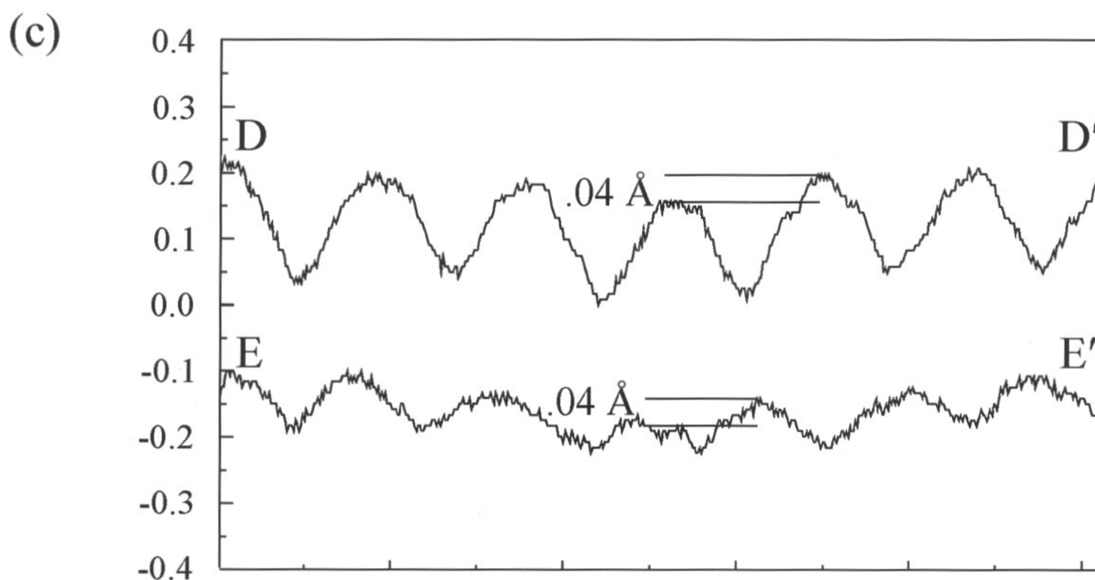
(c)
0.4
0.3
0.2
0.1
0.0
-0.1
-0.2
-0.3
-0.4
D
D′
.04 Å
E
E′
.04 Å

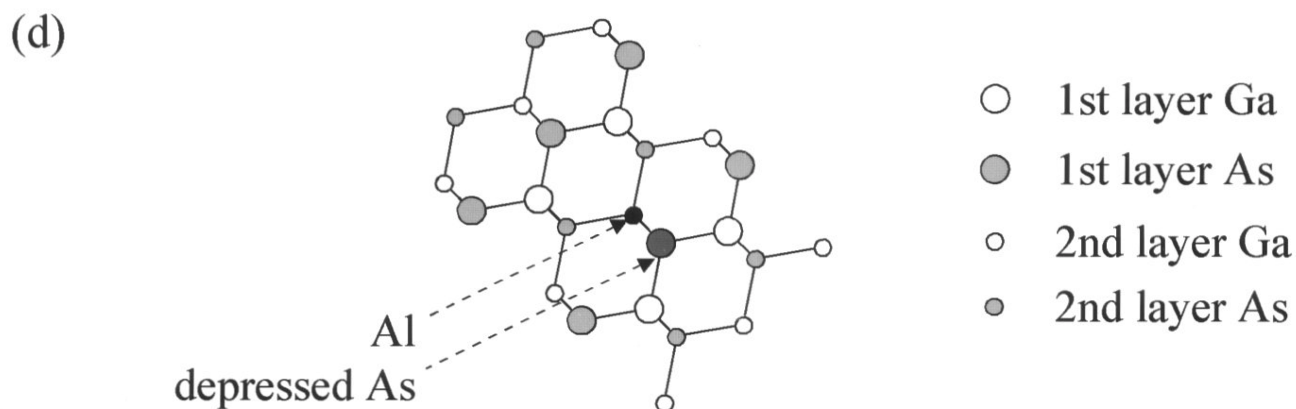
(d)
1st layer Ga
1st layer As
2nd layer Ga
2nd layer As
Al
depressed As

neither of these two features appears outside of the AlGaAs region, we conclude that these are aluminum atom related. There are also a number of what appear to be defect-related features within the AlGaAs region. For example, single arsenic vacancies appear towards the upper right of the image (indicated by "**V**"). These only appear to occupy more than a single site due to the high contrast we have used in this image to bring out the **A** and **B** features more clearly.

Figure 7a shows a zoom-in view of one of the **A** features. Not only does this feature consist of two enhanced atom sites, but also two slightly depressed atom sites, all of which are in almost perfect registry with the arsenic sublattice. This is evident also in the line cut from point A to point A' which shows that, for the tunneling parameters used here, the enhanced arsenic atoms have an apparent height of 0.15 Å relative to the surrounding arsenic atoms (line cut BB') while the depressed arsenic atoms have an apparent height of -0.04 Å relative to the surrounding arsenic atoms (line cut CC'). The mirror symmetry about a $(\bar{1}10)$ plane of this feature is also evident.

Since we are imaging the arsenic sublattice, it is straightforward to conclude that the **A** feature is only consistent with a substitutional atom occupying a first layer site of the gallium sub-lattice. Only in that case would we expect to see an even number of arsenic atoms affected since we know that the (110) surface of GaAs consists of gallium and arsenic atoms that alternate along the $[\bar{1}10]$ direction. Furthermore, since aluminum atoms substitute for gallium atoms, we conclude that these **A** features represent the effect of a first layer aluminum atom.

In our earlier work on AlAs/GaAs short period superlattices (Smith *et al*., 1995a, 1995b), we found that regions of pure AlAs appeared only dark relative to the GaAs regions in the filled state image, while in current work, isolated aluminum atoms appear to have this bright/dark appearance. One possibility is that this appearance is related to a specific physical state of the STM tip. A second possibility is that the surface Al atoms are decorated by certain residual gas atoms such as hydrogen. Detailed calculations would be necessary in order to examine these possibilities. Nonetheless, the symmetry of the feature makes its identification as the effect of a first layer aluminum atom unambiguous.

A similar symmetry argument also allows us to identify that feature **B** is related to the location of the second layer Al atom. Figure 8a shows a zoom-in view of one of the dark sites indicated as **B** in Figure 6. A non-linear gray scale which enhances this feature is also shown in Figure 8b, and line profile across the dark site shows that it is only weakly depressed by about 0.03 Å relative to surrounding arsenic atoms (Fig. 8c). Since only a single arsenic atom is affected, we know that it cannot be the result of an aluminum atom on the first layer because of the lattice symmetry. Therefore, it must be the effect of an aluminum atom occupying the back-bonded, second layer site of the gallium sub-lattice (Fig. 8d).

The ability to identify different chemical constituents in the substitutional alloys opens up the possibility to investigate whether or not a tenary alloy (such as AlGaAs) is random, as favored by entropy, or if instead it is ordered due to atomic-scale interactions during the growth process. Such a question is addressed through the investigation of the Al-Al pair distribution in the GaAs matrix. This function is defined as the probability $p(\mathrm{r})$ of finding a pair of aluminum atoms separated by a certain distance r. $p(\mathrm{r})$ can be obtained from a given spatial distribution of aluminum atoms by calculating the distances between all possible pairs of aluminum atoms and plotting these results in the form of a histogram.

Figure 9 shows the results of an analysis performed for the second layer aluminum atoms labeled in Figure 6. The area has a 30×30 lattice sites with 26 **B** features, corresponding to a concentration of about 3%. The resulting pair distribution histogram is shown in Figure 9 with x's for the plotting symbols. The corresponding theoretical pair distribution histogram (the average of 1000 histograms based on 1000 randomly generated data sets having an average of 26 aluminum atoms) is shown in filled circles. As can be seen, there is fairly good agreement between the experimental and random distributions. However, near the 150 Å pair distance, the experimental points dip slightly below the theoretical points while near the 75 Å pair distance, they rise slightly above them. Analysis of the first layer Al-related features shows a similar behavior. These deviations from a random distribution suggest an Al-Al interaction in the GaAs matrix.

In this analysis, we treated the pair distribution as a function of the pair distance r. In principle, one can investigate this pair correlation as the function of vector r which takes into account the dependence on crystallographic orientation. Such an analysis will undoubtedly provide a much more detailed understanding of the atom-atom interactions. Inevitably, it will require a much larger experimental data base which we have not yet been compiled. However, we expect that such studies will have important implications on the subject of atomic processes in the formation of substitutional alloys.

Mapping Local Optoelectronic Properties Using Near-Field Scanning Optical Spectroscopy

As one of the major applications of semiconductor heterojunctions is in optoelectronics, it is well-motivated to develop a nanometer scale probe to study the opto-electronic properties. Renaud and Alvarado (1991) have developed the technique of tip-induced luminescence (TIL) and have successfully applied it to study AlGaAs/-GaAs heterostructures. The TIL technique involves injection of excess carriers (e.g., electrons) at the tunnel junction and the transport of these carriers to the bulk region followed by the recombination with majority carriers of the opposite type.

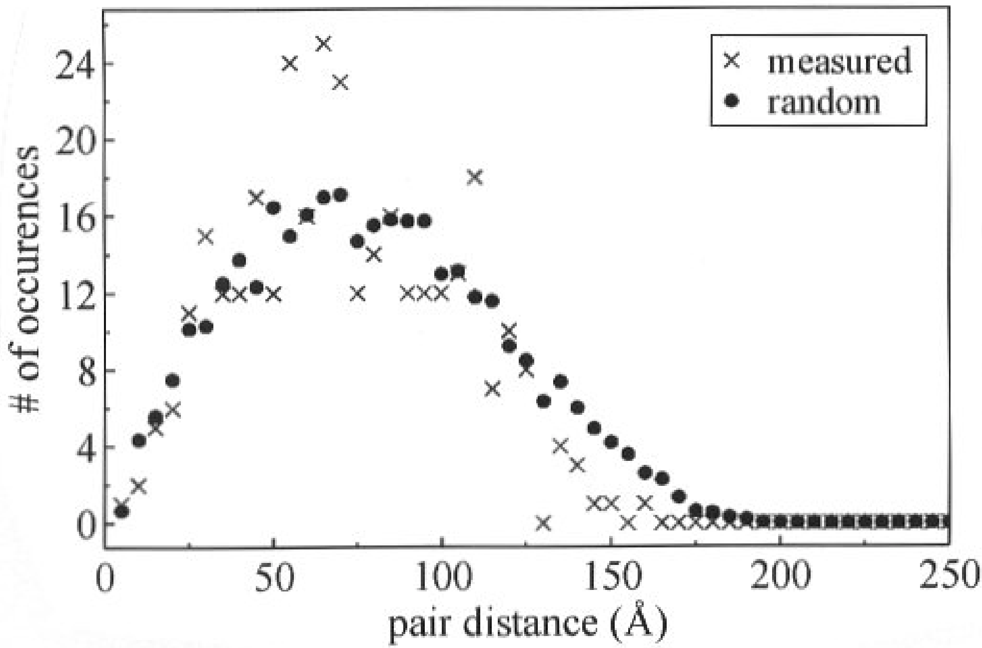

Figure 9. Pair distri-bution histograms for the experimentally-measured and randomly-generated point distributions for the second layer aluminum atoms. The bin size is every 5 Å. This histogram is related to the pair distribution function by a probability normalization factor. The ratio between the actual pair distribution function and the theoretical pair distribution function of a random alloy is also known as the pair correlation function.

While Renaud and Alvarado (1991) have demonstrated high spatial resolution in the luminescence mapping, it still lacks the energy-resolved information of the photon being emitted.

Here, we describe an alternative nanoscale opto-electronic probe utilizing a near field scanning optical microscope (NSOM). Since photons are used as the excitation source of excess carriers, one can study semi-insulating samples which are not accessible using tunneling technique. Furthermore, the finite penetration depth of photons (for both the excitation and emission photons) allows one to probe the buried heterostructures using a top-view geometry which has been nicely demonstrated by Hess *et al.* (1994). The studies presented here, nevertheless, still use the cross-sectional geometry and all the microscopy and spectroscopy studies were performed at room temperature.

The design of our instrument is different from most of the current designs of NSOM. Rather than using the shear-force feedback mechanism to control the tip-sample distance, our design uses the reflected light intensity directly for feedback control. The NSOM tip is made out of a pulled single mode fiber with Al-coating, and is used for local illumination. The typical effective aperture is about 500 Å. Two multi-mode optical fibers each with a numerical aperture of 0.45 were used to collect the photons in reflection geometry. One of the collection fibers is dedicated to detect the reflected light intensity for feedback control. The other collection fiber is coupled to a spectrometer and a liquid nitrogen cooled, back-illuminated, charge collection device (CCD) array to detect the luminescent spectra. This design allow us to arbitrarily choose any operation point in the near-field regime for feedback control. We typically pick an operation point at about 300 Å above the surface. The topographic image acquired using this feedback mechanism is therefore a "constant reflection image" analogous to a constant current image in STM. The details of this design and its performance has been described elsewhere (Guttroff *et al*., 1996). Here we concentrate on its application to studies of AlGaAs/GaAs heterostructure.

Figure 10 shows NSOM topography of a sulfide-passivated cross-sectional surface of AlGaAs/GaAs heterostructures acquired at the constant reflection intensity mode. The contrast in this mode can be due to a combination of true topographic variation and the variation in the local reflectivity. Based on the studies described in **A Direct Mapping of Electronic Structure in Real Space**, we know that the variation of the true surface topography from AlGaAs to GaAs is less than 10 Å for our sulfide passivated sample. On the other hand, the apparent topographic contrast between AlGaAs and GaAs in this constant reflection intensity image is on the order of 100 Å. This contrast is interpreted as due to the difference in the refractive index between AlGaAs and GaAs. The refractive indices of GaAs and $Al_{0.3}Ga_{0.7}As$ are 3.59 and 3.385 respectively. By using a crude approximation of $R = \{(n-1)/(n+1)\}^2$, where R is the reflectivity and n is the refraction index, we obtain the result that the reflectivity of GaAs is about 10% higher than that of $Al_{0.3}Ga_{0.7}As$. One can then explain that the topography in the $Al_{0.3}Ga_{0.7}As$ region is higher because the tip needs to retract to compensate the loss in the reflectivity in the constant reflection mode.

Corresponding to this NSOM image, spatially resolved near-field PL spectra were also obtained. Figure 11a shows

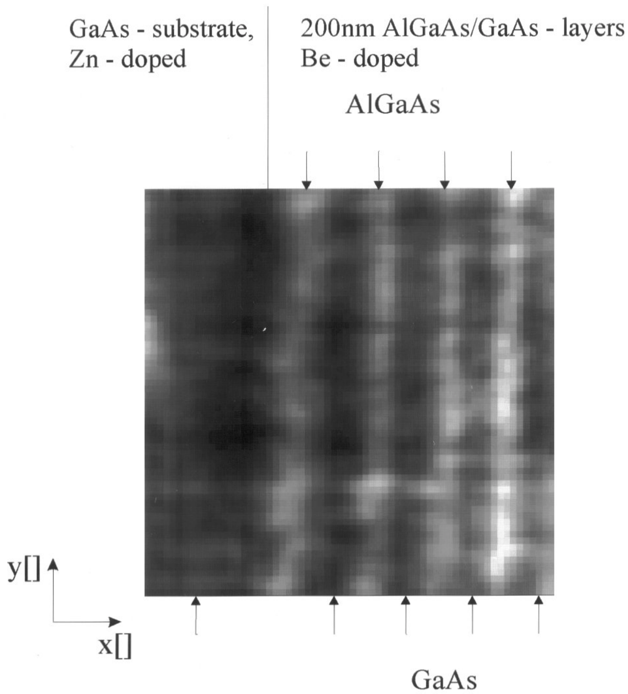

Figure 10. Near-field optical microscopy image of GaAs/AlGaAs multilayers on top of GaAs substrate acquired at a constant reflection intensity mode. Each GaAs and AlGaAs layer is 2000 Å wide.

---

the wavelength resolved near-field PL spectra as a function of the lateral scanning position. Also shown in Figures 11b and 11c are two representative spectra in the substrate and epilayer regions, respectively. There are two major peaks observed in the spectra: one results from the band-to-band transition (conduction band edge energy minus valence band edge energy) (E_c - E_v) of GaAs at $\lambda = 8710$ Å (1.424 eV) and the other one is due to the conduction band edge to the acceptor level transition (E_c - E_a). The peak position of this acceptor related feature changes from $\lambda = 8950$ Å (1.386 eV) in the GaAs substrate region to $\lambda = 8910$ Å (1.392 eV) in the superlattice region. This implies that the binding energy of the Zn-acceptor level is 6 meV higher than that of the Be-acceptor level.

In the superlattice region, the dominant contribution is due to the radiative recombination that occurs in the GaAs region since the photo-generated excess electrons in the AlGaAs region will migrate to the GaAs region. The largest spatial variation in the PL intensity does not show the same periodicity as the superlattice. More likely, this variation in the PL intensity is influenced by local metallurgical imperfections, such as interfacial roughness. On the other hand, we also observe that the intensity ratio between the Be-related peak and the band-to-band peak (E_c - E_v) remains constant in the super-lattice region. We interpret this as due to a constant acceptor concentration in the GaAs layers of the super-lattice region. In the substrate region, the PL intensity decreases near the interface between the substrate and the epi-layer. This is probably due to the existence of an oxide layer on the substrate surface before the epitaxial growth. This oxide layer has a high defect density and, therefore, decreases the radiative recombination efficiency. The intensity ratio of the Zn-related peak relative to the band to band peak (E_c - E_v) is higher in the substrate region than that in the superlattice region. The Zn-related feature is about 6 times stronger than the Be-related feature. This result is also consistent with the concentration of the acceptors.

These spectroscopic studies, while being performed only at room temperature, have already shown the ability to resolved how metallurgical defects influence the luminescence efficiency and the ability to determine the binding energy of p type dopants and their variation in concentration in nanometer scale. Much greater opportunities open up when near-field luminescent spectroscopy can be performed at low temperature. At lower temperature, the intrinsic luminescent quantum efficiency is greatly enhanced as well as the energy resolution of the spectroscopy. The high energy resolution distinguishes small fluctuations of energy levels involved in an optoelectronic transition. Consequently, small inhomogeneity in heterostructure either in composition, quantum size or strain, can all possibly be reflected by near-field luminescent spectroscopy. Such a capability has already been demonstrated in a quantum well system by Hess *et al.* (1994).

Summary

In summary, we have investigated the compound semiconductor heterostructures using various forms of scanning probe microscopy. Cross-sectional scanning tunneling spectroscopy allows one to directly map out the electronic structure. Band offsets, and detailed band structures in AlGaAs/GaAs heterostructure systems have been resolved in real space. Cross-sectional scanning tunneling microscopy provides a true atomic scale view of interfacial roughness. Chemical identifications of different isovalent elements allow us to investigate the atom-atom correlation in the substitutional alloys, thus, opening the potential to have a detailed understanding of atomic processes in the growth of semiconductor alloys. Near-field scanning optical microscopy shows the refractive index contrast between AlGaAs and GaAs. Furthermore, near field scanning photoluminescence spectroscopy reveals the influence of metallurgical defects on the local luminescent efficiency. An important future direction will be to use near-field luminescent spectroscopy and cross-sectional scanning tunneling microscopy to study

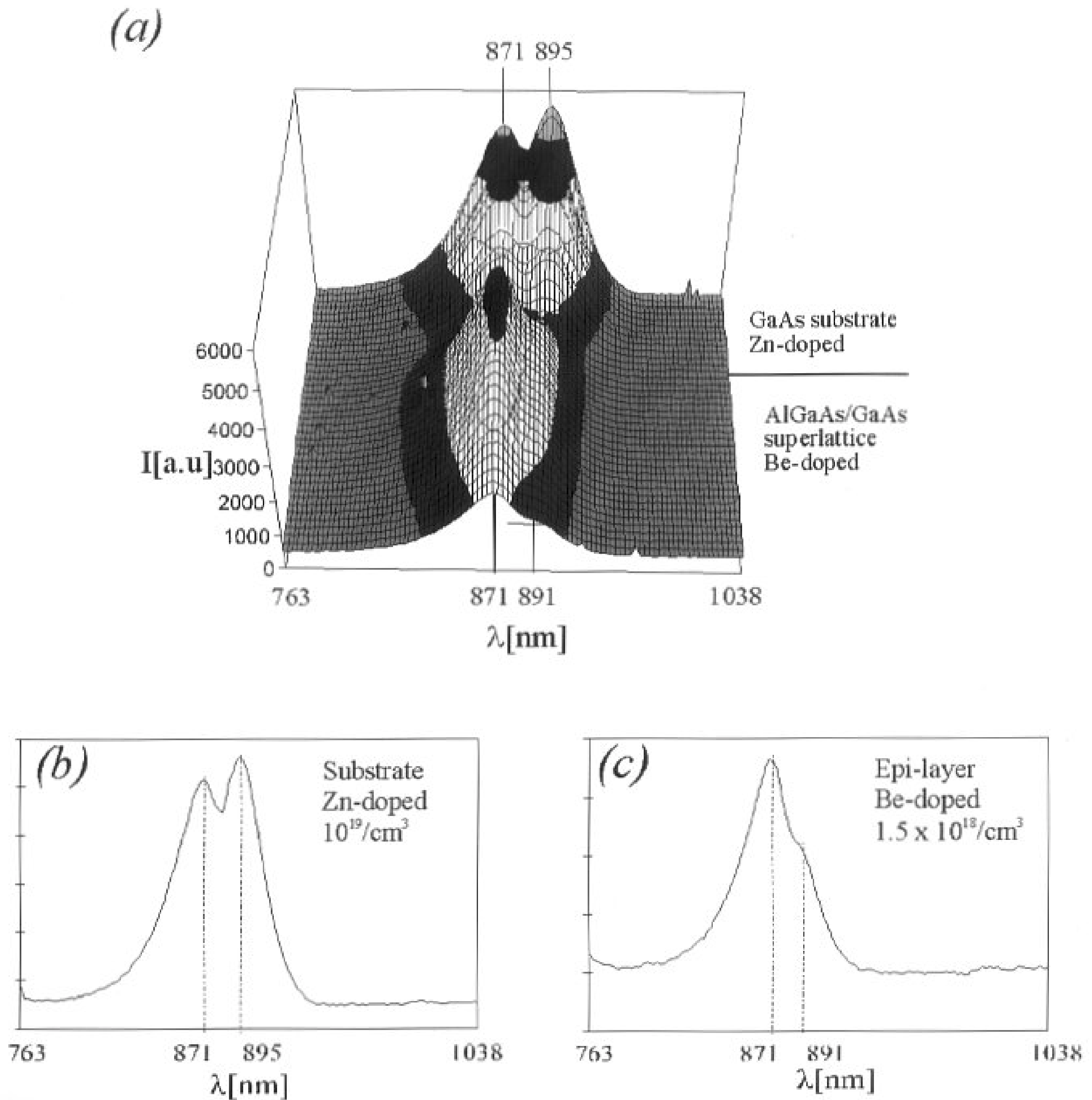

Figure 11. (**a**). Photoluminescent spectra acquired as a function of scanning position across the substrate and multilayer region shown in Figure 10. The z axis scale represents the intensity which is proportional to the photon counts of the CCD-camera. (**b**) and (**c**). Two representative spectra at substrate and the epilayer regions, respectively.

the same quantum heterostructure system, thus, correlating the atomic structure, electronic structure and optoelectronic properties at different length scale.

Acknowledgments

We thank Professor B.G. Streetman and his students at the Microelectronics Research Center at the University of Texas for providing us AlGaAs/GaAs and InGaAs/GaAs heterostructure samples. This work was supported by NSF-DMR 94-02938 and NSF-Science and Technology Center, Grant No. CHE8920120.

References

Albrektsen O, Arent DJ, Meier HP, Salemink HWM (1990) Tunneling microscopy and spectroscopy of molecular beam epitaxy grown GaAs-AlGaAs interfaces. Appl. Phys. Lett. **57**, 31-33.

Chao K-J, Smith AR, Shih CK (1996a) Direct determination of exact charge states of surface point defects using scanning tunneling microscopy: The case of As-vacancy on GaAs(110). Phys. Rev. B **53**, 6935-6938.

Chao K-J, Smith AR, Shih CK (1996b) Application of scanning tunneling microscopy to determine the charge state of surface point defects. J. Vac. Sci. Technol. B **14**, 948-952.

Dagata JA, Tseng W, Bennett J, Schneir J, Harary HH (1992) Imaging of passivated III-V semiconductor surfaces by a scanning tunneling microscope operating in air. Ultramicroscopy **42**, 1288-1293.

Feenstra RM (1994) Tunneling spectroscopy of the (110) surface of direct gap III-V semiconductors. Phys. Rev. B **50**, 4561-4570.

Feenstra RM, Stroscio JA, Tersoff J, Fein AP (1987) Atomic-selective imaging of the GaAs(110) surface. Phys. Rev. Lett. **58**, 1192-1195.

Feenstra RM, Vaterlaus A, Yu ET, Kirchner PD, Lin CL, Woodall JM, Pettit GD (1993) Cross-sectional scanning tunneling microscopy of GaAs doping super-lattices: Pinned vs. unpinned surfaces. In: Semi-conductor Interfaces at Sub-Nanometer Scale. Salemink HWM, Pashley MD (eds.). NATO ASI Series E **243**. Kluwer, Dordrecht, Netherlands. pp. 127-132.

Feenstra RM, Collins DA, Ting D Z-Y, Wang MW, McGill TC (1994) Interface roughness and asymmetry in InAs/GaSb superlattices studied by scanning tunneling microscopy. Phys. Rev. Lett. **72**, 2749-2752.

Guttroff G, Keto J, Shih CK, Anselm A, Streetman BG (1996) A design of reflection scanning near-field optical microscope and its application to AlGaAs/GaAs heterostructures. Appl. Phys. Lett. **68**, 3260-3262.

Gwo S, Chao K-J, Shih CK, Sadra K, Streetman BG (1993) Direct mapping of electronic structure across $Al_{0.3}Ga_{0.7}As$/GaAs heterojunctions: Band offsets, asymmetrical transition widths, and multiple-valley band structures. Phys. Rev. Lett. **71**, 1883-1886.

Hess HF, Betzig E, Harris TD, Pfeiffer LN, West KW (1994) Near-field spectroscopy of the quantum constituents of a luminescent system. Science **264**, 1740-1745.

Johnson MB, Maier U, Meier H P, Salemink HWM (1993a) Atomic-scale view of AlGaAs/GaAs heterostructures with cross-sectional scanning tunneling microscopy. Appl. Phys. Lett. **63**, 1273-1275.

Johnson MB, Albrektsen O, Feenstra RM, Salemink HWM (1993b) Direct imaging of dopants in GaAs with cross-sectional scanning tunneling microscopy Appl. Phys. Lett. **63**, 2923-2925.

Lew AY, Yu ET, Chow DH, Miles RH (1994) Scanning tunneling microscopy of InAs/GaInSb super-lattices. Appl. Phys. Lett. **65**, 201-203.

Pfister M, Johnson MB, Alvarado SF, Salemink HWM, Marti U, Martin D, Morier-Genoud F, Reinhart FK (1995) Indium distribution in InGaAs quantum wires observed with scanning tunneling microscope. Appl. Phys. Lett. **67**, 1459-1461.

Renaud P, Alvarado SF (1991) Mapping quantum-well energy profiles of III-V heterostructures by scanning-tunneling-microscope-excited luminescence. Phys. Rev. B **44**, 6340-6343.

Salemink HWM, Albrektsen O (1993) Atomic-scale composition fluctuations in III-V semiconductor alloys. Phys. Rev. B **47**, 16044-16047.

Salemink HWM, Albrektsen O, Koenraad P (1992) Tunneling spectroscopy across GaAs/$Al_xGa_{1-x}As$ interfaces at nanometer resolution. Phys. Rev. B **45**, 6946-6949.

Smith AR, Chao K-J, Shih CK, Shih YC, Streetman BG (1995a) Cross-sectional scanning tunneling microscopy study of GaAs/AlAs short period superlattices: The influence of growth interrupt on the interfacial structure. Appl. Phys. Lett. **66**, 478-480.

Smith AR, Chao K-J, Shih CK, Shih YC, Anselm A, Streetman BG (1995b) The influence of various growth parameters on the interface abruptness of AlAs/GaAs short period superlattices. J. Vac. Sci. Technol. B **13**, 1824-1829.

Smith AR, Chao K-J, Shih CK, Anselm A, Streetman BG (1996) Identification of first and second Al atoms in dilute AlGaAs using cross-sectional scanning tunneling microscopy. Appl. Phys. Lett. **69**, 1214-1216.

Stroscio JA, Feenstra RM, Fein AP (1987) Local state density and long-range screening of absorbed oxygen atoms on the GaAs(110) surface Phys. Rev. Lett. **58**, 1668-1671.

Zheng JF, Liu X, Newman N, Weber ER, Ogletree DF, Salmeron M (1994) Interface segregation and clustering in strained-layer InGaAs/GaAs heterostructures studied by cross-sectional scanning tunneling microscopy. Phys. Rev. Lett. **72**, 1490-1493.

Discussion with Reviewer

J.W.P. Hsu: The authors use a unique method to regulate NSOM tip-sample distance. Please comment on how different

this method is compared to the commonly used shear force feedback. For example, how far is the tip from the surface during the scan? How sensitive is this feedback method?
Authors: The typical tip-to-sample distance is 300 Å. The determination of the tip-to-sample distance has been described in details in our earlier publication (Guttroff *et al*., 1996) and is therefore not repeated here.

J.W.P. Hsu: The shear force feedback was introduced to keep tip-sample distance constant in NSOM experiments. Using the reflected light intensity for feedback control can introduce artificial topography, as shown in this paper. For GaAs and AlGaAs, which indices are well known, the topographic and optical information can be separated afterwards. How can this feedback method be used to study materials with uncharacterized optical properties and with large topographic changes?
Authors: The referee is correct that the reflection feedback does not give a constant tip-to-sample distance when scan over regions of different refrative indices. This is indeed the effect we use to distinguish between GaAs and AlGaAs regions. We, however, have also tested this designed on surfaces with large topographic changes such as Si-grating. The result was also reported in detail in Guttroff *et al*. (1996).